Green Chemistry

PAPER

View Article Online
View Journal

Cite this: DOI: 10.1039/d6gc01028h

Production of polyols from sugars in biorenewable alcohol: selectivity of hydrogen transfer on metal catalysts

Qiaozhi Zhang,[a,b] Zhuoyue Liu,[a] Xuan Li[a] and Iris K. M. Yu *[a,b]

Received 16th February 2026,
Accepted 5th May 2026

DOI: 10.1039/d6gc01028h

rsc.li/greenchem

Non-H_2 hydrogen donors, such as alcohols, should be explored for their potential to enhance flexibility in hydrogenation reactions, particularly in contexts where alcohols can be produced *via* fermentation from biowaste. This study investigates the aqueous-phase catalytic transfer hydrogenation (CTH) of glucose to sorbitol, revealing the mechanism of isopropanol (IPA) activation as a liquid H donor over a carbon-supported Ru (Ru/C) catalyst. The surface characterization of the catalysts and mass spectra of sorbitol obtained in deuterated solvents suggest that glucose is hydrogenated through the transfer of two equivalent chemisorbed H atoms (H*) on metallic Ru^0, instead of the Meerwein–Ponndorf–Verley mechanism. The co-generation of H_2 gas hints that H* atoms are susceptible to combination among themselves instead of transferring to glucose. An expanded kinetic model including H–H combination as a parallel step to sorbitol formation can qualitatively predict CTH at varying reactant concentrations. The competition between H_2 formation and substrate reduction could vary with the Ru metal nanostructure and substrate energetics: Ru/Al_2O_3 can largely suppress H_2 in glucose CTH, whereas the H selectivity in maltose-to-maltitol CTH is double that in glucose-to-sorbitol. This study demonstrates a renewable H source that can serve as a safer alternative to the pressurized H_2 used in conventional hydrogenation. More importantly, it informs the rational design of catalysts by pinning down the significance of H–H combination, which should be moderated to improve H atom economy in chemical upgrading using non-H_2 reducing agents.

Green foundation

1. This work details the mechanism of glucose-to-sorbitol hydrogenation in isopropanol (IPA) as a liquid hydrogen donor, offering a greener and more renewable alternative to pressurized H_2 gas used in conventional approach.
2. The findings suggest that the reaction proceeds through the metal-mediated transfer of two equivalent chemisorbed H atoms (H*) from IPA to glucose. However, sorbitol formation can suffer from the preferential combination of two H* adatoms to form H_2(g), which behaves as a parallel reaction that competes with glucose for H*. Such a phenomenon resembles the challenge of low faradaic efficiencies in the electroreduction of CO_2 and organic compounds, underscoring that H transfer selectivity is of broad interest to systems relying on non-H_2 hydrogen sources.
3. Future work should explore strategies that suppress H–H combination, *e.g.*, by engineering metal crystallography, to increase the selectivity of H addition to organic substrates.

1. Introduction

Utilizing biomass as a renewable carbon source to replace conventional petroleum-derived feedstocks has attracted increasing attention, driven by the global demand for renewable energy and carbon neutrality. Glucose, the most abundant unit in biomass, can be valorized into a variety of value-added chemicals such as acids and polyols.[1–3] The hydrogenation product sorbitol has broad applications including food, personal care, and pharmaceuticals,[4] while its production relies on H_2 gas in conventional practice. Catalytic transfer hydrogenation (CTH) is an emerging reduction strategy that replaces molecular H_2 with liquid-phase H donors, such as alcohols and organic acids.[5] By avoiding the use of pressurized H_2, CTH mitigates safety concerns and reduces costs associated with H_2 transportation, process equipment, and plant operation. Moreover, it potentially improves the sustainability of industrial processes because those organic H donors can be obtained from renewable resources, for instance,

[a]*Department of Civil and Environmental Engineering, National University of Singapore, Singapore 117576, Singapore. E-mail: irisyu@nus.edu.sg*
[b]*NUS Environmental Research Institute, National University of Singapore, Singapore 117411, Singapore*

through the fermentation of waste rice straw and other biomass.[6,7]

The literature has focused on metal-catalyzed CTH for substrates with furan or aromatic rings (*e.g.*, furfural and guaiacol), which formed the basis of most mechanistic understanding to date. In general, CTH can proceed through metal hydride transfer, in which O–H and α-C–H of alcohols can be activated on metallic sites, donating two equivalent H adatoms that subsequently attack the substrate;[8,9] or through Meerwein–Ponndorf–Verley (MPV) reduction, where the H from O–H is captured by a base or a metallic site, followed by a concerted H transfer from the remaining α-C–H to the substrate by forming a ring intermediate with a Lewis acid site.[8] The assignment of mechanisms can be complicated when catalysts carry both metallic and Lewis acid sites. The MPV mechanism mediated by Ru oxides has been reported to prevail over Ru-based catalysts for the CTH of furan-containing substrates, such as hydroxymethylfurfural[10] and furfural,[11] while metallic Ru catalyzed hydrogenolysis of the CTH products in these systems.

Polyol production from sugars *via* CTH is yet to be thoroughly investigated. Due to structural differences, it is questionable whether the CTH mechanisms of furanic/aromatic substrates apply to sugars. In the Ru-catalyzed CTH of cellulose and glucose, whether the active sites are cationic Ru species ($Ru^{\delta+}$)[12] or metallic Ru sites[13] remains controversial. To be specific, $Ru^{\delta+}$ species are present on carbon-supported Ru (Ru/C) catalysts, which have been suggested to be the active sites in the CTH of cellulose to sorbitol and mannitol.[12] This disagrees with the study of glucose CTH, where metallic Ru in Ru/C was reported to enable the metal hydride mechanism based on the proton NMR spectra of sorbitol products obtained in deuterated solvents.[13] We believe that the advancement of heterogeneous catalysts should be built on a deeper understanding of such a complex system, elucidating the activation of alcohol H donors along with meticulous assignment of active sites.

This study investigates the CTH mechanism of glucose to sorbitol over a Ru/C catalyst in isopropanol (IPA) as the H donor. Our findings support that glucose CTH mainly follows metal-mediated H transfer, where IPA releases two equivalent H* adatoms that subsequently attack glucose. We developed a kinetic model informed by kinetic isotope effects (KIEs) and calibrated against experimental data over a range of glucose and IPA concentrations. This model can explain the volcano-shaped dependence of sorbitol yield on glucose concentration and the stoichiometric excess of acetone, which has been seldom highlighted in the literature. Apart from reaffirming the event of H_2 formation, the kinetic model established in our study emphasizes its competitive relationship with substrate hydrogenation. Accordingly, we proposed possible strategies to improve H selectivity and/or sorbitol production in CTH, including catalyst support design and a hydrogenation-first route from maltose. The findings suggest that H atom economy could be a potential focus area in future research advancing CTH catalysts.

2. Experimental section

2.1 Chemicals and catalysts

Chemicals used in this study mainly include D-(+)-glucose (99.5%, Aladdin), D-fructose (99%, Aladdin), D-(+)-xylose (99%, Aladdin), D-(+)-maltose monohydrate (98.0%, Aladdin), D-glucose-1-^{13}C (99 atom% ^{13}C, Sigma-Aldrich), IPA ($(CH_3)_2CHOH$, 99.9%, Sigma-Aldrich), IPA-d1 ($(CH_3)_2CHOD$, 98 atom% D, Sigma-Aldrich), IPA-d8 ($(CD_3)_2CDOD$, 99 atom% D, Yuanye), *tert*-butanol (99.7%, Sigma-Aldrich), and D_2O (99.9 atom% D, Sigma-Aldrich). Water (18.2 MΩ·cm) was obtained from a water purification system (Milli-Q). Ru supported on carbon (Ru/C, 5 wt% Ru, Macklin) and alumina (Ru/Al_2O_3, 5 wt% Ru, Riogen) were commercial catalysts.

2.2 Glucose CTH reaction

In a typical run of the glucose CTH reaction, 16 mg of glucose, 16 mg of catalyst, and 4 mL of H_2O/IPA mixture (1 : 1 v/v) were added to a glass vial, unless otherwise stated. Herein, IPA was employed as both the H donor and solvent for glucose CTH, whereas water, as the greenest solvent, was introduced as a co-solvent to improve glucose solubility. A pristine catalyst was used for all CTH experiments unless otherwise stated. Then, the vial was placed in a microwave reactor (Monowave 400, Anton Paar, pressure error ±2 bar) for reaction. For reactions at a larger scale using another reactor (flexiWAVE, Milestone), the solution volume was increased to 10 mL, alongside a proportional increase in substrate and catalyst loadings. The reactions followed a temperature program including a ramping stage with a ramping rate of 10 °C min^{-1}, followed by a holding stage at the designated temperature (the holding time in this stage is defined as reaction time). It should be noted that the ramping time of the reactions for kinetic model establishment was minimized to ~0.5 min to obtain the initial reaction rates. The reacted solid–liquid mixture was separated using a 0.45 μm mixed cellulose ester membrane filter. The solid (the spent catalyst) was vacuum dried at 50 °C for 6 h and reserved for characterization studies.

2.3 Product identification and quantification

The concentrations of compounds in the liquid sample were typically quantified using a high-performance liquid chromatography (HPLC, LC-2050C, Shimadzu) system equipped with an HPX-87H (Bio-Rad) column at 65 °C, using 5 mM H_2SO_4 as the mobile phase at a flow rate of 0.4 mL min^{-1}. During glucose CTH over Ru/C, the major by-products were fructose from isomerization (<1.5 Cmol%) and degradation products including glycolic acid (<1 Cmol%) and formic acid (<1 Cmol%). Since this work focuses on hydrogenation and the yields of these by-products were negligible, their detailed product distribution is not shown. For reactions using fructose as the substrate, sorbitol was quantified using a HiPlex-Ca column (Agilent) operated at 80 °C with water as the mobile phase at a flow rate of 0.6 mL min^{-1}. The molecular weights of isotope-labeled compounds were identified by mass spectrometry in the electrospray ionization mode (ESI-MS, LCQ

Fleet ion trap mass spectrometer, Thermo Scientific) using a mobile phase consisting of methanol and water at a volume ratio of 80 to 20. Following CTH experiments under selected conditions, the gas in the headspace of the glass vial (*i.e.*, reactor vessel) was analyzed using a gas chromatography (GC, Agilent 6890) system equipped with an HP-PLOT Molesieve column (Agilent 19095P-MS0) and a thermal conductivity detector (TCD).

2.4 Characterization of catalysts

Particle size distribution and lattice spacing in catalysts were determined from transmission electron microscopy (TEM, JEM-F200, JEOL) images and selected area electron diffraction (SAED) ring patterns. The crystalline phases were determined by X-ray diffraction (XRD, Ultima IV, Rigaku). Lewis acid sites were quantified based on Fourier transform infrared (FTIR) spectroscopy (Tensor 27 FTIR Spectrometer, Bruker) after chemisorption and desorption of pyridine (pyridine-FTIR) at temperatures of 120, 150, and 180 °C; samples were pretreated at 350 °C under vacuum conditions before pyridine sorption. The near-surface chemical states and coordination environment of Ru were analyzed by X-ray photoelectron spectroscopy (XPS, K-Alpha X-ray photoelectron spectrometer, Thermo Scientific) and extended X-ray absorption fine structure (EXAFS, Shanghai Synchrotron Radiation Facility), respectively. *In situ* FTIR (Nicolet iS50 FTIR spectrometer, Thermo Scientific) was used to probe surface species during IPA activation (gas flow rate was fixed at 50 mL min^{-1} during both pre-stabilization and holding stages). Nuclear magnetic resonance (NMR, VNMRS 600 MHz NMR spectrometer, Agilent) was used to determine H spectra in spent catalysts.

2.5 Chemical treatments of the Ru/C catalyst

H_2 reduction of pristine catalysts was conducted at 400 °C for 2 h in a tube furnace using forming gas (5% H_2 in N_2); the reduced catalysts were collected for designated CTH experiments and characterization. Oxidized catalysts were prepared by oxidizing pristine catalysts (1 g of catalyst dispersed in 15 mL of water) using 0.5 mL of 6 wt% H_2O_2 aqueous solution. The mixture was agitated at room temperature for 10 min, followed by vacuum filtration and oven-drying at 105 °C for 2 h.

3. Results and discussion

3.1 Glucose CTH to sorbitol with IPA as a H donor over Ru/C

The preliminary screening test compares glucose CTH catalyzed by Ru/C in the presence of different alcohols as hydrogen donors. The results show that the system with IPA as the hydrogen source produced a significantly higher sorbitol yield than those with other alcohols, including methanol, ethanol, 1-propanol, and 2-butanol, with various alkyl chains and hydroxyl group positions (Fig. S1). Since the literature has discussed the dehydrogenation activities of various H donors,[14,15] the current study adopts a different perspective by investigating chemical events involving multiple reacting species on the catalyst surface. The following CTH experiments were all performed using IPA as the H donor (as schemed in Fig. 1a).

Ru-catalyzed glucose CTH in IPA was conducted under broader conditions. At a reaction time of 20 min, the sorbitol yield increased with temperature up to 140 °C but decreased at higher temperatures probably due to over-reaction (Fig. 1b). The time course at 140 °C shows that the sorbitol yield increased with time and reached a plateau at 82.8 Cmol% within 20 min (Fig. 1c). It should be noted that the increasing trend in acetone production over time provides direct evidence of IPA dehydrogenation at O–H and α-C–H positions. A control experiment in a mixture of *tert*-butanol ($(CH_3)_3COH$) and water (140 °C, 10 min) did not produce sorbitol, suggesting that β-C–H was unlikely to be a H source. The lack of C=C-containing

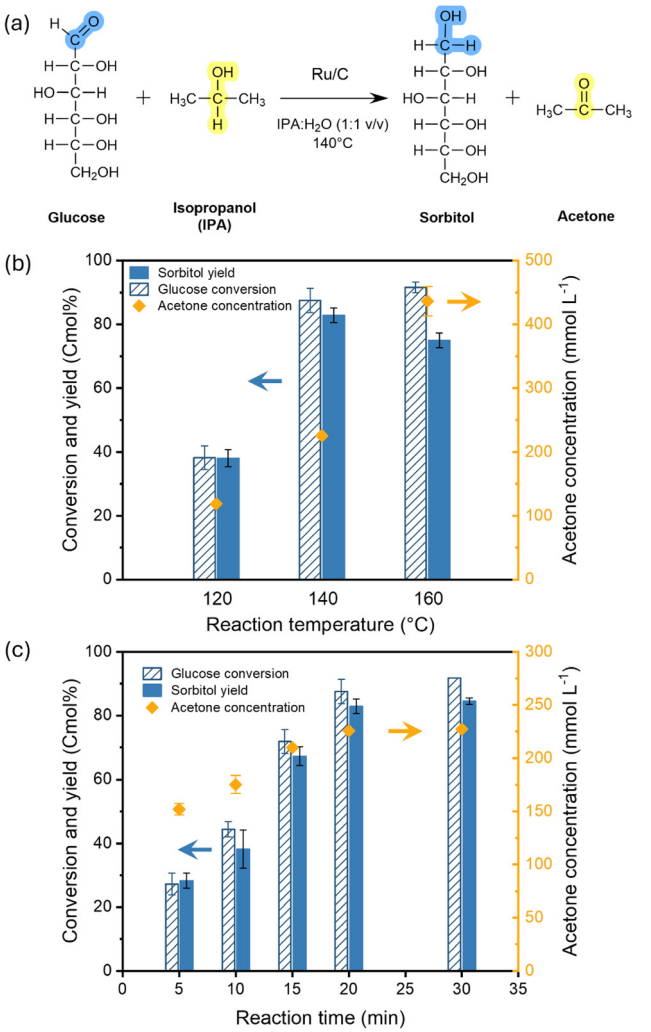

Fig. 1 (a) Scheme of glucose CTH to sorbitol conversion with IPA as the H donor; glucose CTH over the Ru/C catalyst: (b) various temperatures within 20 min and (c) time course at 140 °C (reaction conditions: 16 mg of glucose, 16 mg of Ru/C, 2 mL of IPA and 2 mL of water; Monowave 400).

compounds in the product analysis further suggests a low probability of hydrogen transfer from the β-C–H and α-C–H positions of IPA. Instead, scission at O–H and α-C–H of IPA represents a more feasible route. The question comes down to how H atoms can be transferred from IPA to glucose. Two pathways are widely discussed: the metal hydride (or H adatoms) route that requires a H-bonded metal surface[16,17] as well as MPV reduction that involves the concerted intermolecular H atom transfer *via* a six-membered ring transition state facilitated by Lewis acid.[11] Considering that these pathways are characterized by the participation of distinct active sites (*i.e.*, metals or Lewis acids), the Ru/C catalyst was subjected to detailed analyses.

The analysis of the lattice spacing observed in TEM images and SAED ring patterns reveals both Ru and RuO_2 crystals in pristine Ru/C, although they cannot be observed in XRD due to the nanosize of 2.3 ± 0.2 nm on average (Fig. 2a and b). The EXAFS spectrum of Ru in Ru/C lies between those of Ru foil (metallic Ru^0) and RuO_2 standards, indicating an average valence state between 0 and +4 (Fig. 2c), which is complemented by the R-space results and wavelet transform analysis hinting at the co-existence of Ru–Ru and Ru–O/C bonding (Fig. 2d and e). This agrees with the Ru 3p XPS spectral deconvolution, suggesting 76% cationic $Ru^{\delta+}$ and 24% Ru^0 on the catalyst surface (Fig. 2f). The Ru oxides might account for the Lewis acid site amount of 15–48 μmol g^{-1} measured by pyridine-FTIR spectroscopy at 120–180 °C (Fig. 2g). As both metallic sites and Lewis acid sites were found on Ru/C, neither metal hydride (or H adatoms) transfer nor the MPV step can be excluded from the glucose CTH mechanism at this point.

To identify the prevailing hydrogen transfer route, we first searched for signals of hydride Ru–H. The possible Ru–H signals in the range of −8 ppm to −17 ppm (ref. 16–19) are absent from the ^{1}H NMR spectra of IPA-treated catalysts (Fig. 3a), whereas the *in situ* FTIR spectra of Ru/C under IPA flow shows no peak at ∼1632 cm^{-1} that is typically assigned to Ru–H[20] (Fig. 3b), presenting no evidence of metal hydride formation. Nevertheless, the emerging peaks at 1720 and 1740 cm^{-1} of the *in situ* FTIR spectra could be assigned to the stretching vibrations of C═O of acetone,[21,22] suggesting that IPA can be rapidly activated on Ru/C and dehydrogenated to form acetone. When feeding an IPA–water mixture to Ru/C during *in situ* FTIR analysis (simulating the reaction solvent in CTH experiments), the formation of acetone remains noticeable. The results evidence feasible IPA activation on Ru/C catalysts. In addition, we observed that the reaction vessels remained pressurized (4–6 bar) even after cooling to *ca.* 40 °C, indicating the formation of non-condensable gas after glucose CTH (Fig. S2a). Such a gas product was confirmed to be H_2 by GC analysis (Fig. S3). Molecular H_2 might emerge from the combination of two chemisorbed-H atoms (H*) that result from IPA activation on the Ru surface. This process is analogous to the Tafel step ($2H^* \rightarrow H_2$) in the hydrogen evolution reaction. Therefore, while we may not expect a strong Ru–H bond, the formation of chemisorbed H* on Ru and thus its participation in glucose CTH appear highly plausible.

3.2 Pathway of H transfer to glucose and the active site

It is possible that glucose CTH proceeds through hybrid, sequential H* transfer and MPV reduction. To examine the potential contribution of MPV reduction, glucose CTH was performed in a mixture of H_2O and fully deuterated IPA (IPA-d8); the latter is assumed to exist as IPA-d7 due to facile H/D exchange between the H_2O solvent and the –OD group in IPA. If CTH constitutes an MPV step, the α-C–D bond of IPA-d7 is expected to donate the D atom directly to glucose through the formation of the MPV complex, resulting in sorbitol carrying at least one D atom (*i.e.*, C1-D; non-exchangeable with H from H_2O) (Fig. 4a). However, the ESI-MS profile of sorbitol obtained in H_2O/IPA-d7 (solvent **1**) shows a dominant signal at *m*/*z* 205, which corresponds to sorbitol without any D (adduct of $[C_6H_{14}O_6 + Na]^+$) (Fig. 4b). Such a profile highly resembles that of sorbitol from the control, *i.e.*, H_2O/IPA (without D; solvent **2**). These results rule out the possibility of direct D transfer from the α-C–D of IPA to glucose. In essence, both H atoms (or both H and D atoms) were very likely to be chemisorbed on the catalyst surface before attacking glucose. It should be noted that any D* adatoms would be prone to H/D exchange with H_2O and become H*, accounting for the absence of D atoms in sorbitol derived in H_2O/IPA-d7.

To verify the absence of the MPV step, glucose CTH was performed in D_2O/IPA-d1 (solvent **3**); if MPV took place, the resulting sorbitol would have received one H atom at the C1 position (non-exchangeable) from the α-C–H of IPA-d1. Such a possibility was not supported by the ESI-MS results, which show highly similar profiles of sorbitol obtained in solvent **3** and the fully deuterated medium, D_2O/IPA-d8 (solvent **4**; where addition of two D atoms is the only option). In both spectra, a signal of sorbitol-d2 $[C_6H_{12}D_2O_6 + Na]^+$ with the same relative intensity can be observed at *m*/*z* 207 (while sorbitol-d1 at *m*/*z* 206 may result from H/D exchange between sorbitol-d2 and the mobile phase during ESI analysis) (Fig. 4b). This suggests that two D atoms were transferred to glucose in solvent **3** as in solvent **4** regardless of the presence of α-C–H in the former, reaffirming our speculation that MPV is unlikely to occur in this study. This aligns with a previous study that reported the presence of C1–D in sorbitol obtained in a similar catalytic system (Ru/C, D_2O/IPA) based on proton NMR spectroscopy,[13] advocating for the adatom addition path rather than MPV. Our study further shows that such an adatom transfer mechanism prevails in low-water-content CTH of glucose, as evidenced by the similar ESI-MS profiles of products obtained in D_2O/IPA-d1 regardless of the solvent ratio (1 : 1 or 1 : 7 v/v; Fig. S4).

The theory of H* adatom transfer should be underpinned by verifying metallic Ru sites as the active sites in glucose CTH. We altered the relative abundance of the metallic phase by reducing the pristine catalysts in H_2 gas, which was then validated by characterization, as shown in Fig. S5. It is observed that the particles were largely preserved in nanosize (2.6 ± 0.9 nm) after reduction as depicted in the TEM images; thus, the Ru dispersion (50%) was estimated to be comparable with pristine Ru/C (56%) based on the particle-size–dispersion

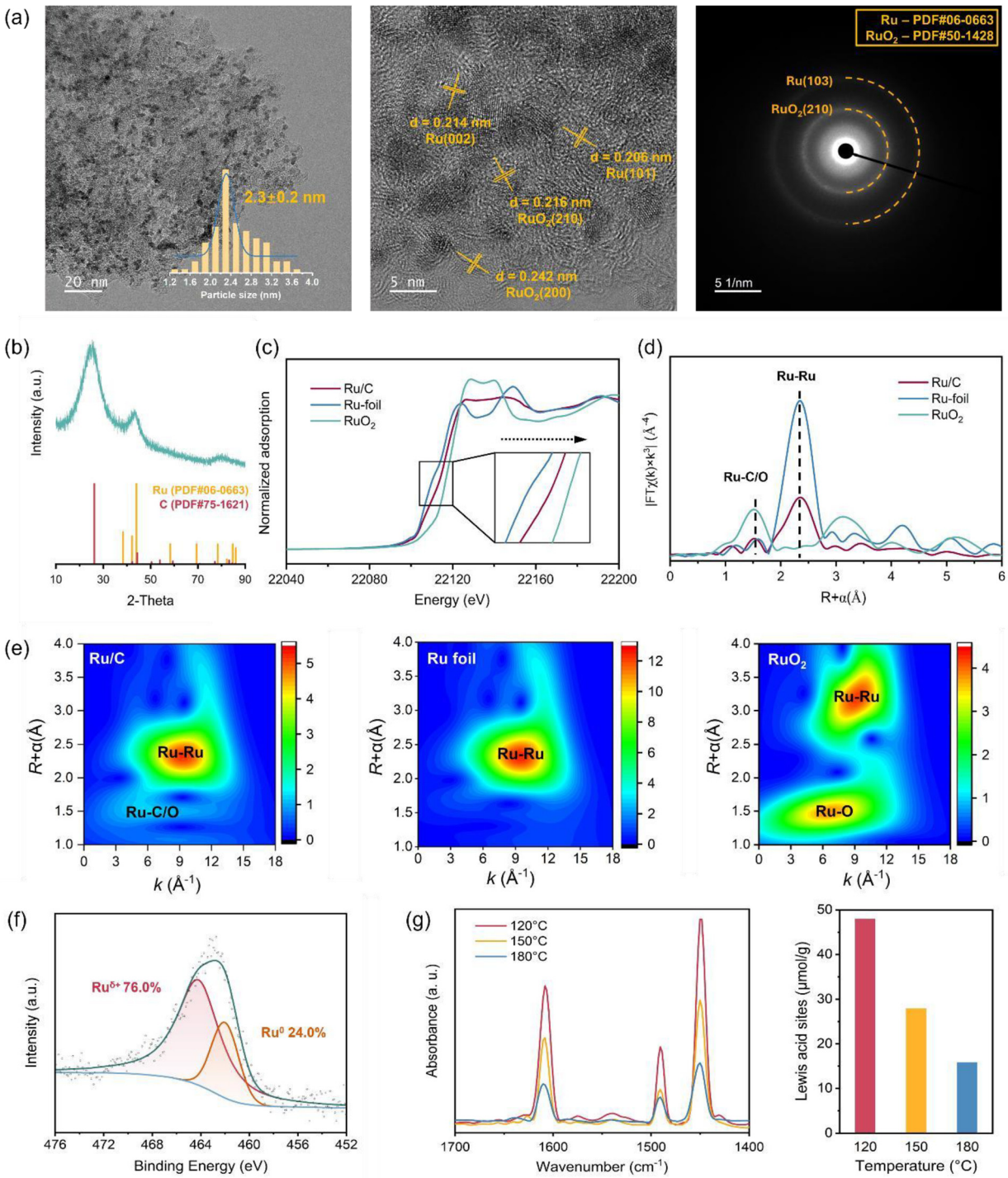

Fig. 2 Characterization of Ru/C: (a) TEM images and SAED ring patterns with typical lattice spacing and particle size distribution; (b) XRD pattern with peak references; EXAFS analysis including (c) *E*-space, (d) *R*-space, and (e) wavelet transform results compared with Ru foil and RuO_2; (f) Ru 3p XPS spectral deconvolution results; and (g) pyridine-FTIR spectra and the corresponding Lewis acid site quantification at various pyridine desorption temperatures.

relationship.[23] The XRD pattern of reduced Ru/C exhibits more prominent diffraction peaks assigned to metallic Ru compared to that of the pristine catalyst. The near-surface chemical states of Ru were analyzed by the curve fitting of the Ru 3p XPS spectra. The proportion of Ru^0 (462.0 eV (ref. 24)) increased from 24.0% to 30.8% after reduction (Fig. 2f & Fig. S5). We remarked that the samples can be partially oxidized when exposed to air during handling, which may account for the

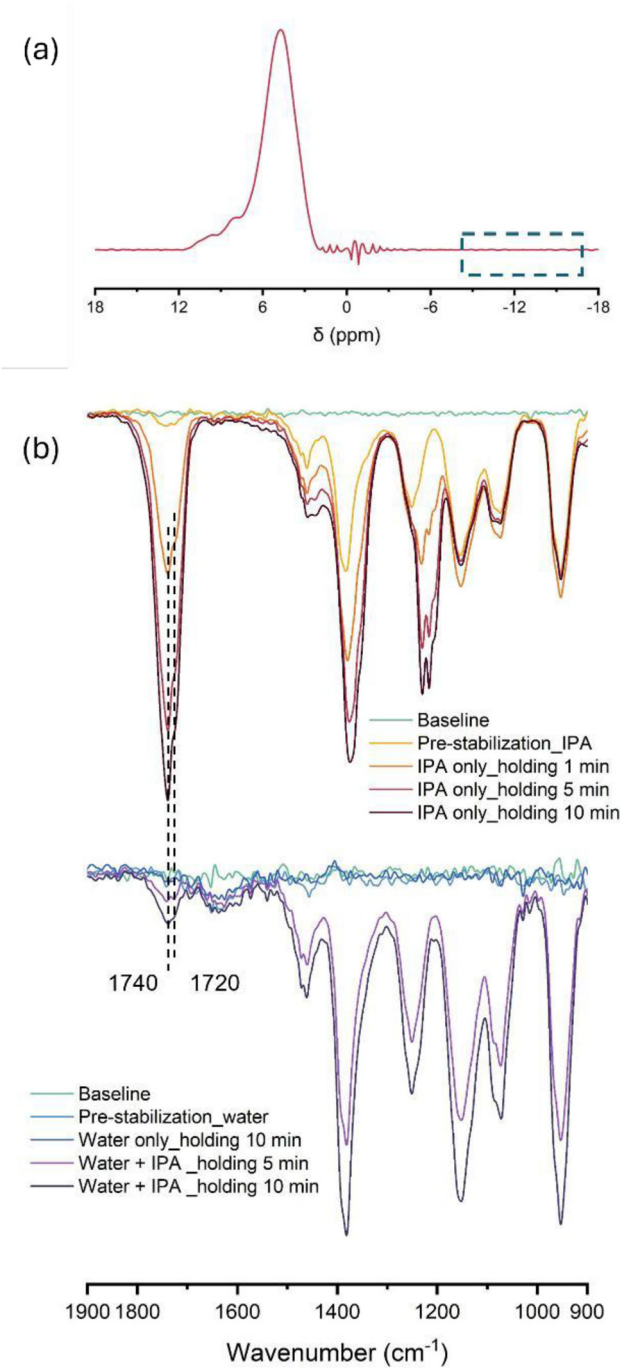

Fig. 3 (a) ^{1}H NMR spectra of IPA-treated Ru/C (treatment conditions: 40 mg of pristine Ru/C, 5 mL of IPA and 5 mL of water at 140 °C for 30 min; flexiWAVE); (b) *in situ* FTIR spectra of Ru/C under the flow of IPA and water only and IPA–water (1 : 1 v/v) mixtures (pre-stabilization temperature: 50 °C, holding temperature: 80 °C; and flow rate of each solvent vapor: 50 mL min^{-1}).

subtle differences in the XPS results. The number of Lewis acid sites on the reduced Ru/C decreased by 20–60% compared to pristine Ru/C (Fig. S6), indicating fewer surface $Ru^{\delta+}$ species, *i.e.*, a higher Ru^{0} content, after reduction, which corroborates the XPS results.

The reduced catalyst was then evaluated in glucose CTH experiment. It is evident that the reduced Ru/C achieved 2.3–2.8 times the sorbitol yield of the pristine catalyst at different temperatures. Because the particle size and dispersion remained comparable before and after reduction, the enhanced performance of glucose hydrogenation can be attributed to the increased fraction of the Ru^{0} phase as the major active sites (Fig. 7a). It is noteworthy that acetone production also triplicated (*e.g.*, 869.3 mmol L^{-1} for reduced Ru/C *vs.* 286.3 mmol L^{-1} for pristine Ru/C at 140 °C), suggesting Ru^{0} species as the active sites for IPA dehydrogenation (to acetone) as well. Combining these observations, we believe that glucose CTH begins with the activation of IPA on metallic Ru to form two H* adatoms (and acetone), followed by two H* addition steps to glucose to form sorbitol.

3.3 Impact of H–H combination on sorbitol formation kinetics

Microkinetic studies were performed for a deeper mechanistic understanding. Kinetic isotope effects (KIEs) were studied to determine if IPA was involved in the kinetically relevant step in glucose CTH over Ru/C. The comparable yields of sorbitol obtained from glucose and glucose-1-^{13}C (Fig. 5a) suggest that C1 of glucose did not participate in the rate-determining step. Conversely, both sorbitol and acetone production decreased while using solvent IPA-d8 (or IPA-d7) that is characterized by α-C–D (*i.e.*, solvents **1**&**4**), compared to IPA (or IPA-d1) that carries α-C–H (*i.e.*, solvents **2**&**3**) (Fig. 5b). This result suggests that the activation of α-C–H (α-C–D) in IPA for H* formation is rate-limiting, which agrees with another CTH system (2,3-diphenylacrylonitrile CTH over a Zn-based catalyst) where the dissociation of α-C–H in methanol was proposed as the rate-determining step.[25]

A kinetic model was then derived featuring the rate-determining IPA activation (equation derivation detailed in Text S1). We first considered the simplest reaction network involving only cascade steps – starting with IPA activation to give two H* atoms that are then added to glucose (Scheme S1). One may expect the rate law to be:

$$\text{Rate of sorbitol formation} = \frac{k_1 K_{IPA} C_{IPA}}{1 + K_G C_G + K_{IPA} C_{IPA}} \quad (1)$$

where K_G and K_{IPA} are the apparent equilibrium constants of glucose and IPA adsorption, respectively; C_G and C_{IPA} are the concentrations of glucose and IPA, respectively; and k_1 is the apparent rate constant of IPA dehydrogenation. It is noteworthy that the rate equation predicts a negative correlation between the sorbitol yield and glucose concentration (C_G), which, however, is contradictory to the results of CTH experiments in varying C_G, at 0–11.1 mmol L^{-1} in particular (Fig. 6b). Specifically, the CTH experimental results show a volcano-shaped pattern of sorbitol production as a function of C_G (Fig. 6b). Such a discrepancy between theoretical prediction and actual observation suggests that a more complex model should be applied.

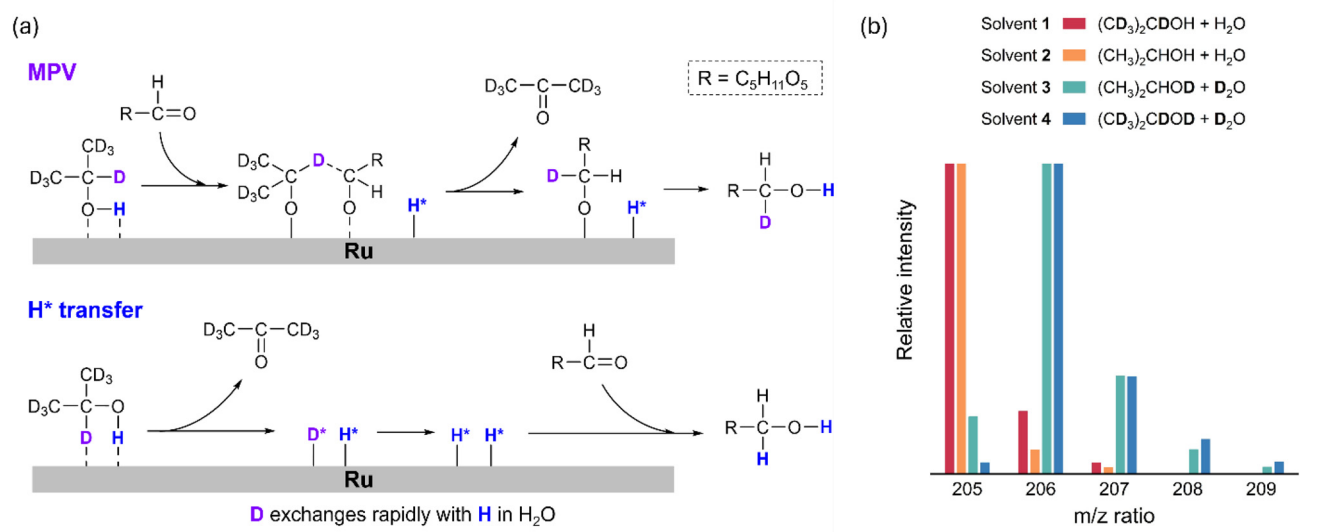

Fig. 4 (a) Two possible mechanisms of glucose CTH to sorbitol in solvent **1** (H donor IPA-d8 assumed as IPA-d7 in H_2O solvent); (b) ESI-MS profile of products from glucose CTH in various D-labelled solvents (reaction conditions: 16 mg of glucose, 16 mg of Ru/C, 2 mL of IPA and 2 mL of water at 140 °C for 10 min; Monowave 400. Assignment of main adducts: *m/z* 205 for $[C_6H_{14}O_6 + Na]^+$, *m/z* 206 for $[C_6H_{13}DO_6 + Na]^+$, and *m/z* 207 for $[C_6H_{12}D_2O_6 + Na]^+$).

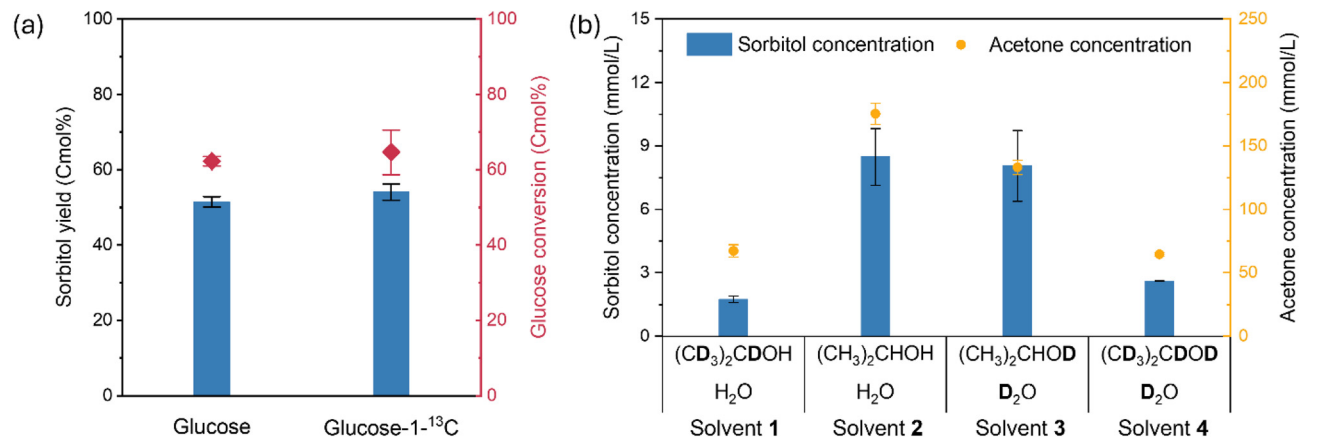

Fig. 5 Effects of (a) ^{13}C at glucose C1 and (b) D-labelled solvents on glucose CTH kinetics (reaction conditions: 16 mg of glucose, 16 mg of Ru/C, 2 mL of IPA and 2 mL of water; Monowave 400; (a) 120 °C for 30 min; (b) 140 °C for 10 min).

We observed that acetone production over Ru/C consistently exceeded the stoichiometric amount by several tens of times (*i.e.*, acetone-to-sorbitol molar ratio ≫1 : 1), hinting that a parallel reaction takes place and produces acetone. This aligns with our observation about H_2 formation (Fig. S2 & S3). The pressure-based estimation of the H_2 gas amount in moles (using the ideal gas law) is close to the missing fraction of the H balance in the CTH reaction (Fig. S2b), suggesting molecular H_2 as the major gaseous product. Lining up these findings, we speculate that upon the dehydrogenation of IPA to acetone, the two released H* adatoms tend to combine with each other on Ru, producing molecular H_2; such a pathway considerably competes with glucose reduction for chemisorbed H* and thus sorbitol formation.

To verify, we expanded the kinetic model by incorporating the competitive H_2 formation step (Fig. 6a) and derived the following rate equation (details of derivation in Text S2):

$$\theta_G = \frac{K_G C_G}{1 + K_G C_G + K_{IPA} C_{IPA}} \quad (2)$$

$$\text{Rate of sorbitol formation} = \frac{r_1 k_2 \theta_G}{k_2' + k_2 \theta_G} \quad (3)$$

where θ_G is the coverage of glucose (eqn 2), r_1 is the rate of IPA (α-C–H) activation (eqn S5), and k_2 and k_2' are the apparent rate constants of sorbitol and H_2 formation, respectively. Experimental rate data and operating parameters (C_G and C_{IPA}) were fitted into the rate equation to approximate apparent

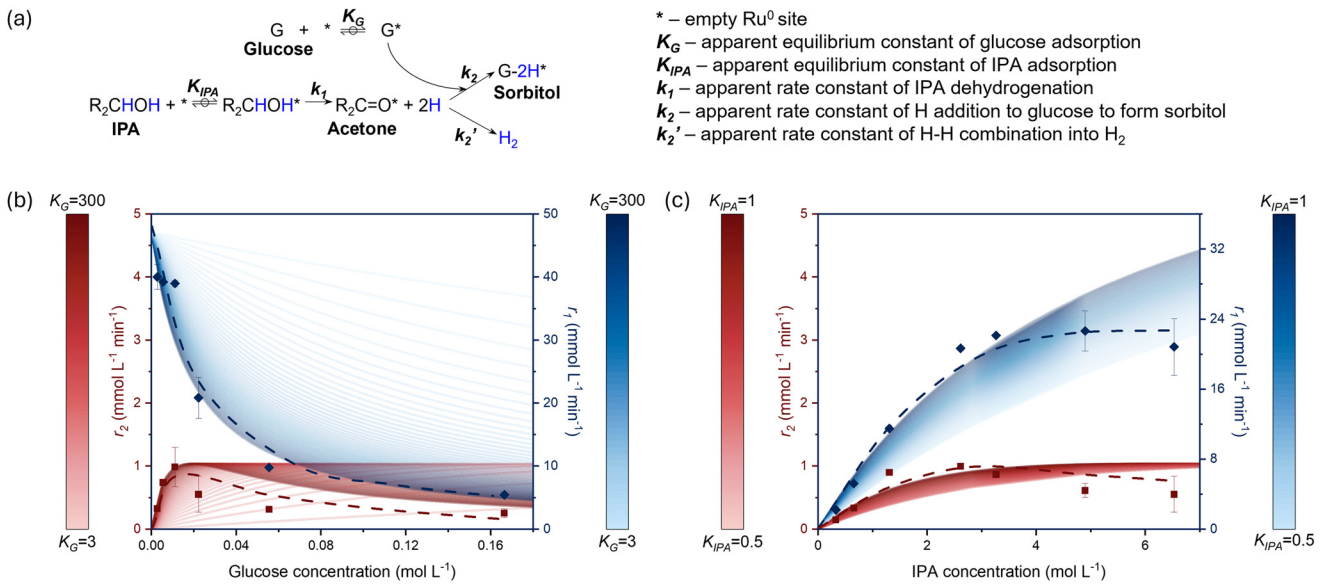

Fig. 6 (a) Proposed scheme for establishing kinetic equations; experimental results (scatter points and dashed trend lines) and predicted trends (solid lines) of the rate of IPA dehydrogenation (r_1) and the rate of H addition to glucose (r_2) as a function of (b) glucose loading in a solvent comprising 2 mL of IPA and 2 mL of water and (c) as a function of IPA concentration at a glucose loading of 16 mg and a total solvent volume of 4 ml (reaction conditions: 140 °C for 5 min; Monowave 400). Predicted trends were obtained using eqn S5 for r_1 and eqn 3 for r_2, where K_{IPA} = 0.726 L mol^{-1} in (b), K_G = 204 L mol–^{1} in (c), k_1 = 5.70 × 10^{-2} mol L^{-1} min^{-1}, k_2 = 7.58 × 10^{-5} mol L^{-1} min^{-1} and k_2' = 8.26 × 10^{-4} mol L^{-1} min^{-1} were optimized using Excel Solver based on experimental data.

equilibrium constants (K_G and K_{IPA}) and apparent rate constants (k_1, k_2, and k_2'). K_{IPA} was assumed to be 1 L mol^{-1} (ref. 26) at the beginning and then optimized together with other constants using Excel Solver. These constants were then used in visualizing the reaction rate patterns, rates as a function of glucose and IPA concentrations, considering a certain range of K values. As shown in Fig. 6b and c, the reaction rate patterns described by the model qualitatively capture the key features of the experimental results. Specifically, acetone decreases and sorbitol production exhibits a volcano-shaped pattern with increasing glucose concentration; changes in both products become less pronounced at high glucose concentrations (Fig. 6b). When increasing IPA concentration, the formation of both acetone and sorbitol shows logarithmic growth in simulation and experiments (Fig. 6c). It is noted that the co-production of H_2 was documented in cellulose CTH systems[12,13] although this was not often discussed in broader CTH studies.

3.4 Potential strategy to enhance CTH

Inspired by the observation that most H* atoms combine to form molecular H_2 rather than being taken up by glucose, we proposed a catalyst design strategy centering on the suppression of H–H combination to increase the formation of reduced organic products. We noted that the sorbitol-to-acetone ratio (approximated as sorbitol-to-H_2 ratio) appears to be constant for Ru/C, regardless of CTH operating conditions and chemical pretreatments (*i.e.*, oxidation and reduction) of the catalysts (Fig. 7a). To test whether this is a generic phenomenon, supplementary glucose CTH experiments were performed using a different catalyst, *i.e.*, Ru/Al_2O_3. Likewise, it exhibits a constant sorbitol-to-acetone ratio and yet is distinct from that of Ru/C. The results imply that the degree of competition for H* (between H_2 and sorbitol formation) can be controlled by more detailed descriptors of catalyst properties other than the oxidation state; such properties could be altered using different supports. A previous study also noted the distinct CTH performances of Ru catalysts on different supports.[12]

Our results show that the sorbitol-to-acetone ratio over Ru/Al_2O_3 is approximately 8 times that of Ru/C, suggesting that the glucose substrate becomes more competitive on Ru/Al_2O_3 in terms of H* uptake (Fig. 7a). We speculate that the Ru sites on these two catalysts have different crystallography (*e.g.*, numbers and types of faces and edges), electron density, and/or ensemble size, as a result of metal–support interactions. Ru alloying may provide a feasible route to tune these characteristics as well. For example, phosphidation to form Ru_2P has been reported to dilute the Ru–Ru ensemble and thus tune Ru characteristics.[27] Computational and experimental studies have shown that the Ru planes, adsorption positions (top and bridge), electron density, and the Ru–Ru ensemble size can affect the adsorption of substrates (*e.g.*, toluene and the CO probe molecule)[27] as well as H binding with a reported range of 0.08–0.48 eV.[28–31]

Tuning adsorption *via* surface engineering might provide a feasible avenue to mitigate H–H combination and alter H transfer selectivity in CTH. Conceptual energy profiles are proposed to illustrate this theory (Fig. 7b and c). On surfaces that allow stronger binding (*i.e.*, lower energy level), the activation energy of H_2 formation would increase, considering that H–H combination is typically *endothermic* and thus has a *late* tran-

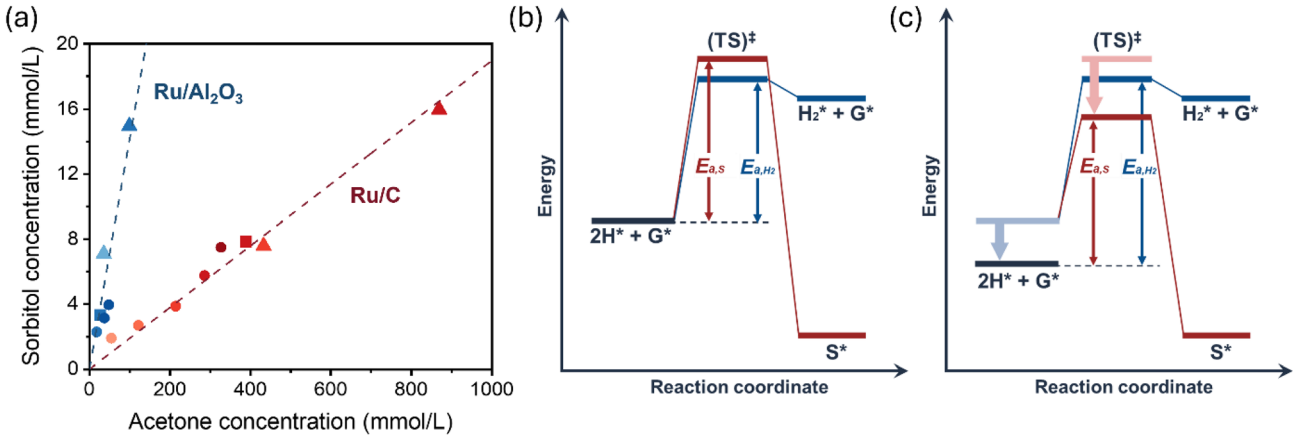

Fig. 7 (a) Correlations between sorbitol and acetone concentrations over different Ru/C and Ru/Al_2O_3 catalysts: pristine – circles, oxidized – squares, and reduced – triangles (reaction conditions: 0.04 g of glucose, 0.04 g of catalyst, 5 mL of IPA and 5 mL of water; reaction temperature range of 80–160 °C – color: from light to dark; 30 min; flexiWAVE); energy profiles of hydrogenation of glucose (G) to sorbitol (S) and H–H combination into H_2 under the hypothetical conditions of (b) weak binding and (c) strong binding of H and glucose on a catalyst surface. E_a – activation energy; TS – transition state.

sition state (as opposed to dissociative H_2 adsorption). In cases where glucose hydrogenation is *exothermic*, which has been supported by theoretical calculations for certain precious metal faces,[32,33] an *early* transition state is presumed. Its energy level might lower along with the reactants to a similar extent, possibly maintaining a constant activation energy of sorbitol formation. We infer that due to such thermodynamic difference (endothermic *vs.* exothermic), strengthening glucose and H binding on the metal surface might slow H_2 formation while sustaining sorbitol formation, leading to a higher apparent rate of the latter.

We futher examined the CTH of more biomass-derived sugars over Ru/C, including fructose-to-sorbitol, xylose-to-xylitol, and maltose-to-maltitol conversion (Fig. 8). In general, this CTH system can be applied to diverse monosaccharides sourced from various natural polysaccharides (*e.g.*, starch, cellulose, and hemicellulose) and disaccharides such as maltose. It is noteworthy that the turnover frequency (TOF) of maltose-to-maltitol CTH was 4.8 times that of the glucose-to-sorbitol system, while the TOF of acetone formation was only 2.4 times, corresponding to the two-fold increase in H transfer selectivity to the polyol product. These results hint at the significant role of substrates in governing H transfer selectivity, in which the adsorption energies and their impact on reaction kinetics should be further studied. Our results also suggest that a sequential hydrogenation–hydrolysis route using readily available maltose syrup may offer higher efficiency and H atom economy in sorbitol production than glucose CTH, which should be verified in future research. Previously reported Ru-based CTH reactions on various biomass-derived substrates (*e.g.*, furfural and guaiacol) are summarized in Table S1. Overall, the reported systems typically required an hour-scale reaction time to achieve high conversion and/or yield; in this study, a minute-scale reaction time was adopted for sorbitol yields ≥80%.

We remark that the low H atom economy in our CTH system resembles the longstanding challenge in electrochemical reduction reactions, where H_2 evolution is considered a side reaction that lowers faradaic efficiency in the electroreduction of CO_2 [34] and larger organic molecules.[35] It appears that H transfer selectivity presents a challenge to broader systems – both thermocatalysis and electrocatalysis – that rely on non-H_2 hydrogen sources, which is worthy of further investigation.

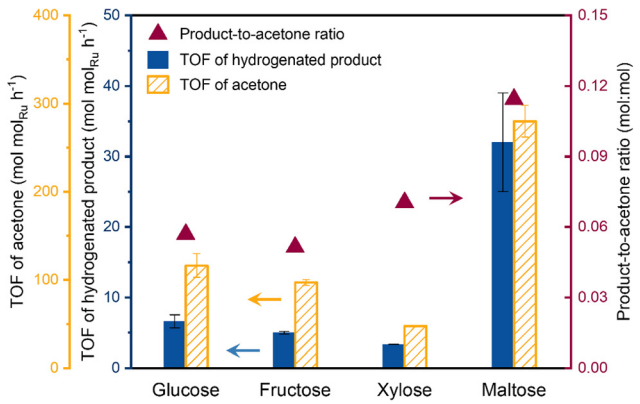

Fig. 8 CTH of glucose, fructose, xylose, and maltose over Ru/C with IPA as the H donor: TOF of formation of hydrogenation products (*i.e.*, sorbitol, sorbitol, xylitol, and maltitol, respectively) and acetone as well as their ratio (reaction conditions: 111 mmol L^{-1} substrate, 16 mg of Ru/C, 2 mL of IPA and 2 mL of water at 140 °C for 20 min; Monowave 400).

4. Conclusion

In summary, we validate a chemisorbed-H (H*) atom transfer mechanism of glucose CTH to form sorbitol over a Ru/C catalyst using IPA as the hydrogen source. On metallic Ru active

sites, the reaction proceeds with the rate-determining activation of IPA, specifically at the O–H and α-C–H positions, releasing two equivalent H* adatoms for supply to glucose. However, the combination of surface H* to form molecular H_2 emerges as a highly competitive H-consuming step in parallel with glucose-to-sorbitol formation; the former should be suppressed to increase H selectivity to sugar alcohols as target products. This mechanistic study deepens our understanding of the transfer and fate of hydrogen in a CTH system, guiding the development of catalysts with higher H atom economy.

Author contributions

Q. Z., Z. L., and X. L. performed the experiments and analyzed the data. Q. Z. wrote the manuscript and prepared the data visualization. I. K. M. Y. reviewed and/or edited the manuscript before submission. All authors contributed substantially to the discussion of the content and the writing of the article.

Conflicts of interest

There are no conflicts to declare.

Data availability

The data supporting this article have been included as part of the supplementary information (SI). The SI file includes additional figures on hydrogen donor screening, H_2 balance and identification, isotope-labeling experiments, and catalyst characterization, as well as a literature comparison table and detailed derivations of the kinetic models used in this study. Supplementary information is available. See DOI: https://doi.org/10.1039/d6gc01028h.

Acknowledgements

The authors acknowledge the financial support provided by Singapore A*STAR MTC Young Individual Research Grant (YIRG) (H24-MRG0887; WBS: A-8003272-00-00).

References

1 J. Install, *et al.*, Selective oxidation of glucose–galactose syrup to gluconic and galactonic acids, *Green Chem.*, 2025, **27**(23), 6725–6733.
2 Z. Xie, *et al.*, Boosting energy efficiency and selectivity of glucose oxidation toward glucuronic acid in high-frequency ultrasound using multicavity CuO catalytic cavitation agents, *Green Chem.*, 2025, **27**(3), 573–585.
3 J. Lee, *et al.*, Catalytic and electrocatalytic conversion of glucose into value-added chemicals, *Renewable Sustainable Energy Rev.*, 2023, **181**, 113337.
4 Y. Zhou, R. L. Smith and X. Qi, Chemocatalytic production of sorbitol from cellulose via sustainable chemistry – a tutorial review, *Green Chem.*, 2024, **26**(1), 202–243.
5 D. Wang and D. Astruc, The golden age of transfer hydrogenation, *Chem. Rev.*, 2015, **115**(13), 6621–6686.
6 X. Shi, *et al.*, Isopropanol production using engineered *Corynebacterium glutamicum* from waste rice straw biomass, *Bioresour. Technol.*, 2024, **396**, 130416.
7 E. Rochón, *et al.*, Bioprocess intensification for isopropanol, butanol and ethanol (IBE) production by fermentation from sugarcane and sweet sorghum juices through a gas stripping-pervaporation recovery process, *Fuel*, 2020, **281**, 118593.
8 M. J. Gilkey and B. Xu, Heterogeneous catalytic transfer hydrogenation as an effective pathway in biomass upgrading, *ACS Catal.*, 2016, **6**(3), 1420–1436.
9 Y. Zhao, *et al.*, Water-assisted catalytic transfer hydrogenation of guaiacol to cyclohexanol over Ru/$NiAl_2O_4$, *Chem. Eng. J.*, 2024, **485**, 149934.
10 J. Jae, *et al.*, The Role of Ru and RuO_2 in the catalytic transfer hydrogenation of 5-hydroxymethylfurfural for the production of 2,5-dimethylfuran, *ChemCatChem*, 2014, **6**(3), 848–856.
11 M. J. Gilkey, *et al.*, Mechanistic insights into metal lewis acid-mediated catalytic transfer hydrogenation of furfural to 2-methylfuran, *ACS Catal.*, 2015, **5**(7), 3988–3994.
12 H. Kobayashi, *et al.*, Transfer hydrogenation of cellulose to sugar alcohols over supported ruthenium catalysts, *Chem. Commun.*, 2011, **47**(8), 2366–2368.
13 A. Shrotri, *et al.*, Transfer hydrogenation of cellulose-based oligomers over carbon-supported ruthenium catalyst in a fixed-bed reactor, *ChemCatChem*, 2014, **6**(5), 1349–1356.
14 B. García, *et al.*, Catalytic transfer hydrogenation of glucose to sorbitol with raney® ni catalysts using biomass-derived diols as hydrogen donors, *ACS Sustainable Chem. Eng.*, 2021, **9**(44), 14857–14867.
15 P. Panagiotopoulou, N. Martin and D. G. Vlachos, Effect of hydrogen donor on liquid phase catalytic transfer hydrogenation of furfural over a Ru/RuO_2/C catalyst, *J. Mol. Catal. A: Chem.*, 2014, **392**, 223–228.
16 S. Revathi and T. Ghatak, Ethanol as hydrogen donor: An efficient transfer hydrogenation of aldehydes, ketones, and nitroarenes with H-bonded Ru(II)-N-heterocyclic iminium complex, *J. Catal.*, 2024, **429**, 115207.
17 Y. Peng, *et al.*, Ru/$Zr(OH)_4$ as a transfer hydrogenation catalyst under additives-free condition, *ChemCatChem*, 2023, **15**(1), e202201132.
18 D. Yang, *et al.*, Formic acid as the H_2-carrier and the transfer hydrogenation reagent for Ru-catalyzed hydroaminomethylation of olefins, *J. Catal.*, 2023, **428**, 115132.
19 A. Kumar, R. Bhardwaj and J. Choudhury, Integrated CO_2 capture and conversion to methanol leveraged by the transfer hydrogenation approach, *ACS Catal.*, 2023, **13**(2), 927–933.
20 L. Ge, *et al.*, Synergistic catalysis of Ru single-atoms and zeolite boosts high-efficiency hydrogen storage, *Appl. Catal., B*, 2022, **319**, 121958.
21 M. Shen, *et al.*, Ni-Foam-structured Ni–Al_2O_3 ensemble as an efficient catalyst for gas-phase acetone hydrogenation to

isopropanol, *ACS Appl. Mater. Interfaces*, 2021, **13**(24), 28334–28347.
22 K. Liu, *et al.*, Intensified gas-phase hydrogenation of acetone to isopropanol catalyzed at metal-oxide interfacial sites, *Chem. Eng. J.*, 2023, **454**, 140059.
23 G. Bergeret and P. Gallezot, Particle Size and Dispersion Measurements, in *Handbook of Heterogeneous Catalysis*, 2008, pp. 738–765.
24 L. Zhu, *et al.*, Ruthenium–nickel–nickel hydroxide nanoparticles for room temperature catalytic hydrogenation, *J. Mater. Chem. A*, 2017, **5**(17), 7869–7875.
25 X. Liu, *et al.*, Enable biomass-derived alcohols mediated alkylation and transfer hydrogenation, *Nat. Commun.*, 2024, **15**(1), 7012.
26 B. Demir, *et al.*, Effects of water on the kinetics of acetone hydrogenation over Pt and Ru catalysts, *J. Catal.*, 2021, **403**, 215–227.
27 S. Furukawa, *et al.*, Remarkable enhancement in hydrogenation ability by phosphidation of ruthenium: specific surface structure having unique Ru ensembles, *ACS Catal.*, 2018, **8**(9), 8177–8181.
28 M. Allés, *et al.*, Atomic Hydrogen interaction with transition metal surfaces: a high-throughput computational study, *J. Phys. Chem. C*, 2024, **128**(47), 20129–20139.
29 C. Onwudinanti, *et al.*, Hydrogen diffusion out of ruthenium—an ab initio study of the role of adsorbates, *Phys. Chem. Chem. Phys.*, 2020, **22**(15), 7935–7941.
30 Y. Li, *et al.*, Crystallinity dependence of ruthenium nanocatalyst toward hydrogen evolution reaction, *ACS Catal.*, 2018, **8**(7), 5714–5720.
31 M. Qiu, *et al.*, Directly converting cellulose into high yield sorbitol by tuning the electron structure of Ru2P anchored in agricultural straw biochar, *J. Cleaner Prod.*, 2022, **362**, 132364.
32 Z. Fang, *et al.*, Machine-learning-assisted catalytic performance predictions of binary alloy catalysts for glucose hydrogenation, *Appl. Catal., A*, 2025, **691**, 120086.
33 Y. Nakata, *et al.*, Theoretical study of cellobiose conversion by supported metal catalysts, *Chem. Phys. Lett.*, 2024, **845**, 141285.
34 H. Ooka, M. C. Figueiredo and M. T. M. Koper, Competition between hydrogen evolution and carbon dioxide reduction on copper electrodes in mildly acidic media, *Langmuir*, 2017, **33**(37), 9307–9313.
35 S. Han and W. T. Choi, Mechanistic understanding of electrochemical hydrogenation of 5-hydroxymethylfurfural (HMF) via scanning electrochemical microscopy (SECM), *Chem. Commun.*, 2025, **61**(38), 6969–6972.